Hole Localization and Ultrafast Electron Transfer Dynamics in $CuInS_2$/Organic Molecule Composite

Jayanta Dana,* Arthur Houplin, and Nikolai V. Tkachenko*

Chemistry and Advanced Materials Group, Faculty of Engineering and Natural Sciences, Tampere University, 33720 Tampere, Finland

E-mail: jayanta.dana@tuni.fi; nikolai.tkachenko@tuni.fi

Abstract

Exploring the dynamics of photoexcited electrons and holes in green I-III-VI ternary quantum dots (QDs) is of utmost necessity to design and improve its functionality and applicability in devices. Here, we have studied the dynamics of photoexcited nascent carriers in $CuInS_2$/ZnS (CISZ) core-shell QDs as a potential excited state electron donors using picosecond time-resolved emission and femtosecond transient absorption (fsTA) spectroscopy techniques. The emission decay measurements conducted in the 460–660 nm wavelength range allowed us to distinguish between emission due to electron-hole recombination at conduction (CB) and valence bands (VB), respectively, and due to recombination of the CB electrons and holes at the self-trapped states (Cu^{1+} centers). The excited state electron transfer (ET) was studied by attaching anthraquinone-2-carboxylic acid (AQ) electron acceptor to the QDs.The ET from the CB of CISZ QD to AQ was confirmed by the fsTA studies, which revealed formation of characteristic anion (AQ^-) band at 600 nm. The ET time constant was estimated to be 1.5 ps in ideal one-to-one CISZ-AQ complex, and the charge recombination takes

place with time constant > 5 ns at delay times beyond the fsTA instrument reach. We propose that such a long lifetime of the charge separated state is achieved after the hole localization at the (Cu^{1+}) defect, which effectively decouples the hole at QD and the electron at AQ.

Introduction

I-III-VI ternary quantum dots (QDs) dragged the attention of photonic research community over II-VI QDs owing to their green nature and unique photophysical behaviors which make them promising materials for solar cells, photocatalysis, light emitting diodes, imaging etc.[1–6] The photophysical properties of the green I-III-VI ternary QDs are quite distinguished from other Cd and Pb chalcogenide-based nanocrystals (NCs). The unusual photophysical properties of the ternary systems regardless of size and composition such as large Stokes shift along with a very broad emission band are due to their complicated lattice structure as two different Cu^{1+} ans In^{3+} cations are involved in the bond.[7,8] Following photoexcitation, the generated electron (e^-) - hole (h^+) pair is involved in different types of photophysical activities including carrier cooling, carrier trapping, and carrier recombination, which control the performance of the QD devices and can be explored by ultrafast transient absorption spectroscopy. The radiative and non-radiative recombination have several manifestations by different spectroscopy techniques such as 1) recombination through band edge (BE) and surface trapped,[9,10] 2) radiative recombination between e^- and trapped h^+,[11,12] 3) radiative recombination between h^+ and trapped e^-,[6,13] 4) recombination through the dark and bright state, etc.[8,14]

The QDs having a very large surface-to-volume ratio are very prone to generate surface traps owing to unsaturated dangling bonds on the surface, and it can be either e^- or h^+ traps, or both depending upon the nature of the surface.[15,16] In addition to this surface state, some intrinsic inter band trapped states are generated in the I-III-VI QDs due to the use of different cation and their stoichiometry ratio which provides a degree of freedom in optimizing

the photophysical properties of these green light antenna materials.[17–19] These states drive the photophysical properties of the I-III-VI QDs, resulting in very broad photoluminescence band with large Stoke's shift.[20–22] The most debated topic of this material is the different types of recombination such as trapping at the surface and intrinsic states, radiative and non-radiative recombinations which are long-term riddles for this type of QDs.

Several controversial explanations for different radiative and non-radiative transitions based on time-resolved emission and absorption spectroscopy measurements were proposed. The pump-probe studies detected both radiative and non-radiative transition due to delocalized e^-–localized h^+ recombination and e^- trapping, respectively.[23] The broad emission was explained by the combination of two distinct transitions such as band edge and surface recombination as explained by Seongkyu et. al.[24] Two different transitions were assigned to excitonic and Cu-related sub-band gap state by Danilo et. al.[22] The in situ photoluminescence spectro-electrochemical measurement were used to determine the radiative recombination between delocalized e^- and the trapped h^+, and simultaneously, both the dark and bright nanocrystals were also detected by the Arjan group.[8] Recently, the temperature and applied magnetic field-dependent photoluminescence studies led to conclusion that the radiative recombination is due to recombination of delocalized e^- and localized h^+ at Cu^{1+} center.[14]

Despite debated unusual photophysical behavior, these ternary green QDs have shown quite good power conversion efficiency in quantum dots-sensitized solar cells and photocatalysis. These green QDs are extensively used in CO_2 reduction in the QDs-metal-porphyrin nanocomposite, where these QDs are used as the light antenna and the e^- donor to activate porphyrin catalyst.[2,25] Despite many assumptions, hypotheses, and several controversial explanations supported by some spectroscopic data on the e^- and h^+ recombination process, there is no common consensus on the mechanism of the reactions. To improve the application of materials in real optoelectronic devices the detailed photophysical studies of these QDs are calling for further investigation to establish the exact phenomena involving e^- and

h^+ after photoexcitation. In addition to this, the charge transfer and charge separation in CISZ-organic molecule donor-acceptor systems have not been explored yet, which is the key to solar energy devices.

In order to establish the origin of broad emission and dynamics of nascent e^- and h^+ in I-III-VI QDs, we have conducted time-resolved absorption and emission spectroscopy measurements of commercially purchased CISZ core-shell QDs. We have resolved different competitive processes of the photoexcited charge carrier in this QD and measured charge transfer processes in QD and anthraquinone-2-carboxylic acid (AQ) composite systems. The decay-associated spectra of conducted time correlated single photon counting (TCSPC) measurement in the 460–630 nm range reveal the h^+ localization at the Cu^{1+} center, and the time constant for this process is found to be 0.5 ns. The long-lived broad red emission was attributed to recombination of delocalized e^- at CB and trapped h^+ at Cu^{1+} center. The performed femtosecond transient absorption (fsTA) measurements distinguished the two simultaneous processes, the hole trapping (HT) and e^--h^+ recombination at the BE, and allowed to estimate their time constants as 570 ps and 330 ps, respectively. Quite strong emission quenching of CISZ in the presence of AQ was shown to be due to the photoinduced electron transfer (ET), as was indicated by a separate band for AQ^- in fsTA spectra of CISZ/AQ composite. The measured ET time constant was found to be ca. 1.5 ps for ideal one-to-one attachment of AQ on QD. In parallel with the ET from the conduction band to AQ, the hole at the valence band is trapped by Cu^{1+} defect state, which results in decoupled of the e^-- h^+ pair and formation of the long-lived charge separation QD^+/AQ^-. Therefore, the resolved different transitions and establishment of charge separated state formation of CISZ QDs with organic molecule have potential to develop advanced optoelectronic devices.

Experimental Section

Materials

The studied materials oleic acid-capped CISZ was purchased from PlasmaChem, Germany. The well-known e^- acceptor anthraquinone-2-carboxylic acid molecule was purchased from Sigma-Aldrich.

Femtosecond transient absorption spectroscopy

All the TA measurements have been carried out in chloroform solvent using a 1 mm cuvette in ambient conditions. Commercial Libra F (Coherent Inc.) laser system generates compressed 800 nm pulses with 1 mJ energy, splitting into two parts. The first one with weak intensity generates a white light continuum (400–750 nm) and 900–1200 nm after focusing 800 nm pulses on a heavy-water cuvette and sapphire crystal, respectively, and was used for the broadband probe. The second harmonic of the laser fundamental was used to excite samples at 400 nm. The pump spot size was larger than the probe diameter. Exci-Pro pump-probe spectrometer (CDP Inc.) was used to perform the measurement. The CCD camera for the visible spectral range (400–750 nm) and NIR (900–1200 nm) was used for data acquisition. Upto 6 ns delay window on the probe line was used. The used pump intensity was sufficiently low to avoid multiple exciton generation.

Results and discussion

Photophysics of isolated CISZ

Figure 1 (A) shows the steady-state absorbance and emission spectra of colloidal CIS/ZnS (CISZ) core-shell QDs solution dispersed in chloroform. The absorbance spectrum is very broad, and it has no sharp exciton peak which is typical for alternative II-VI QDs.[26,27] The broad emission spectrum (FWHM = 100 nm) along with a large Stokes shift can be attributed

to self-trapped emission (STE) rather than to the band edge (BE) emission. It is already reported in the literature that the I-III-VI ternary QDs are defect-oriented materials and the emission is predominantly due to recombination of some intrinsic defect states.[19,28] The normalized TA spectrum for a single exciton just after cooling following 400 nm excitation is shown in Figure 1 (A) along with the absorption and emission spectra. It consists of a bleach (420–500 nm) and a broad photoinduced absorption (PIA) (at $>$ 500 nm). The former corresponds to the BE transition(1S-1S) and confirms the postion of the band gap corresponding roughly 460 nm. The latter can be either defect or excited state absorption. There is a long-term controversy on this PIA and the major literature considers it as an absorption of trapped h^+.[23]

To study the origin of emission which is also on dispute for this QDs, we have used the time-correlated single photon counting (TCSPC) technique with excitation at 405 nm and monitoring the emission decays in the wavelength range from 460 to 640 nm with 20 nm interval. All the decay traces are shown in ESI and decays at two characteristic wavelengths, 460 and 560 nm, are presented in Figure 1 (B). The emission decay at 460 nm corresponds to the BE or direct recombination of the e^- and h^+ at CB and VB, respectively. At this wavelength, virtually no steady-state emission can be seen, but apparently, there is an instant rise of emission which is followed by a fast decay.

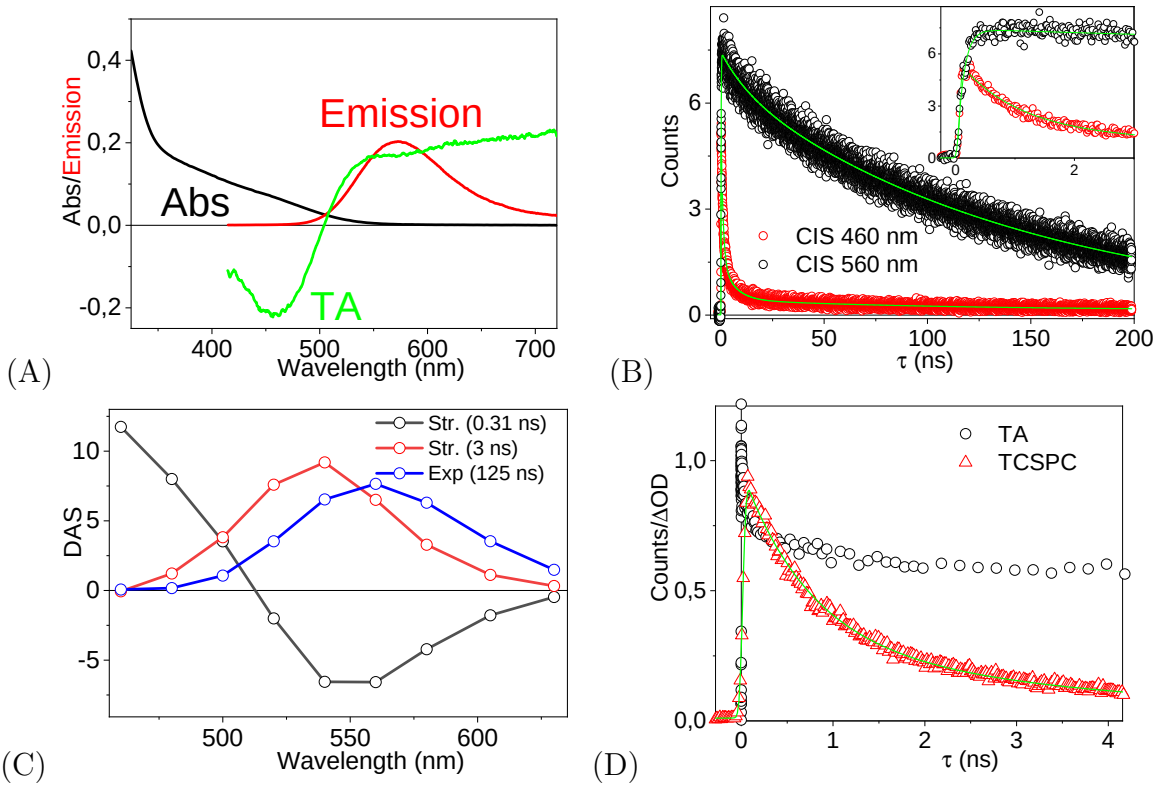

Figure 1: (A) Absorbance, emission and TA (after cooling with 500 fs time constant) spectra of CISZ core shell. (B) TCSPC decay traces of this core-shell at 460 and 560 nm following 405 nm excitation. In inset: Same decay kinetics in an expanded scale. (C) TCSPC global fitted decay associated spectra of CISZ excitation. (D) Comparison of scaled emission and TA decays at the wavelength corresponding to the BE state (roughly 460 nm).

The monitoring wavelength of 560 nm is quite far from the BE emission and can be attributed to the STE. The STE may come out only after e^- or h^+ trapping, and somewhat slower rise was observed, though the rise becomes more obvious after the global fit which delivers decay associated spectra (DAS) shown in Figure 1 (C). To achieve a reasonable quality of the global emission decay fit, we had to use three-component models with two components being stretched-exponential and one exponential (the global $\chi^2 = 1.0327$). The fast stretched component ($\tau = 0.31$ ns and $\beta = 0.43$) has a positive amplitude in the blue part of the spectrum and a negative at $\lambda > 520$ nm. It indicates fast decay of the emission in the blue and a rise in the green-red part of the spectrum as expected. The spectrum of long-lived exponential ($\tau = 125$ ns) resembles very much that of the steady state emission

with maximum around 560 nm. A surprising outcome is the stretched component with $\tau = 3$ ns and $\beta = 0.43$. It has a maximum at around 500 nm and lifetime in between the other two components. We attribute it tentatively to inhomogeneity of our system, such as some variation in size and shape, different number of defects per QD, etc, which cannot be covered by using stretched exponential in place of ordinary exponential. It can be also argued that there are QDs without defects, for which CB e^-- VB h^+ recombination is the only relaxation process, then this component can be attributed to this QDs and its decay rate assigned to k_{eh}. Two possible explanations are trapping of the CB e^- which is followed by the radiative recombination (RR) with the VB h^+, and the VB h^+ trapping by Cu^{1+} defect state which is followed by RR with the CB e^-.[20]

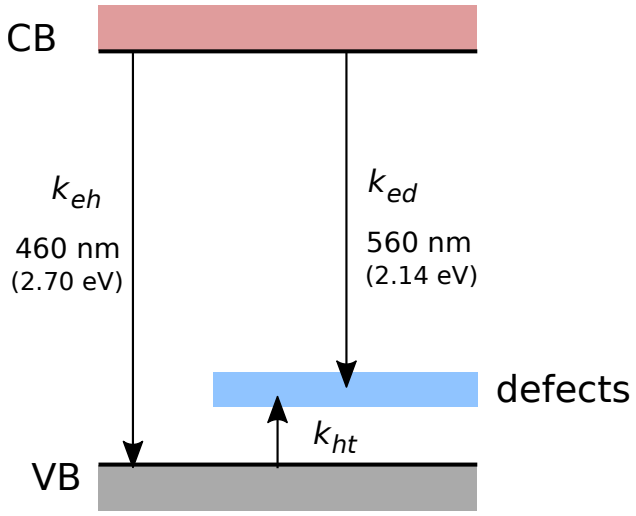

Figure 2: Energy diagram with transitions (see text for details).

The h^+ trapping by Cu^{1+} can be proved by examining TA time profile in the BE wavelength region and comparing it with the emission decay measurements (TCSPC) at 460 nm as shown in Figure 1 (D). The TA response at BE is mostly due to the photo-carriers in the CB. The time resolution of the TA measurements is much better than that of TCSPC and the fast initial decay of the TA signal can be attributed to the photo-carrier thermalization. However, in the range well resolved by both techniques ($>$ 100 ps) the decays of TCSPC and TA kinetics do not follow each other within our pump-probe time window (5 ns). Only

a minor recovery of BE bleaching can be seen within a few ns, suggesting that majority of the CB e^- do not recombine. But the emission at 460 nm depends on both the e^- at CB and h^+ at VB, and it decays almost completely in the same time scale. This means that the emission decay is due to the disappearance of h^+ at the VB, which can be attributed to the h^+ trapping by the Cu^{1+} state.[20]

At the qualitative level the phtoto-dynamics of CSIZ QDs can be explained by the scheme presented in Figure 2. The photo-excitation generates e^--h^+ pair with e^- in the CB and h^+ in the VB. We will assume that the carrier thermalization after the excitation is fast compared to the time scale of TCSPC measurements, ignore it in the scheme. The e^--h^+ pair can recombine with the rate constant k_{eh}. This recombination can produce a photon with energy corresponding to the BE, roughly 460 nm. A competing process is elevation of the h^+ to the defect level with the rate constant k_{ht}, which quenches the emission at 460 nm and opens another recombination process of e^- at the CB and h^+ at the defect level with the rate constant k_{ed}. The latter is observed as a broad emission with maximum close to 560 nm.

Steady state absorbance, emission, and TCSPC of CISZ/AQ composite

To explore the dynamic nature of photoexcited e^- and h^+, we have studied the e^- transfer process of CISZ using a well-known e^- acceptor anthraquinone-2-carboxylic acid (AQ) which is also equipped with two caboxylic acids to promote CISZ-AQ hybride formation.

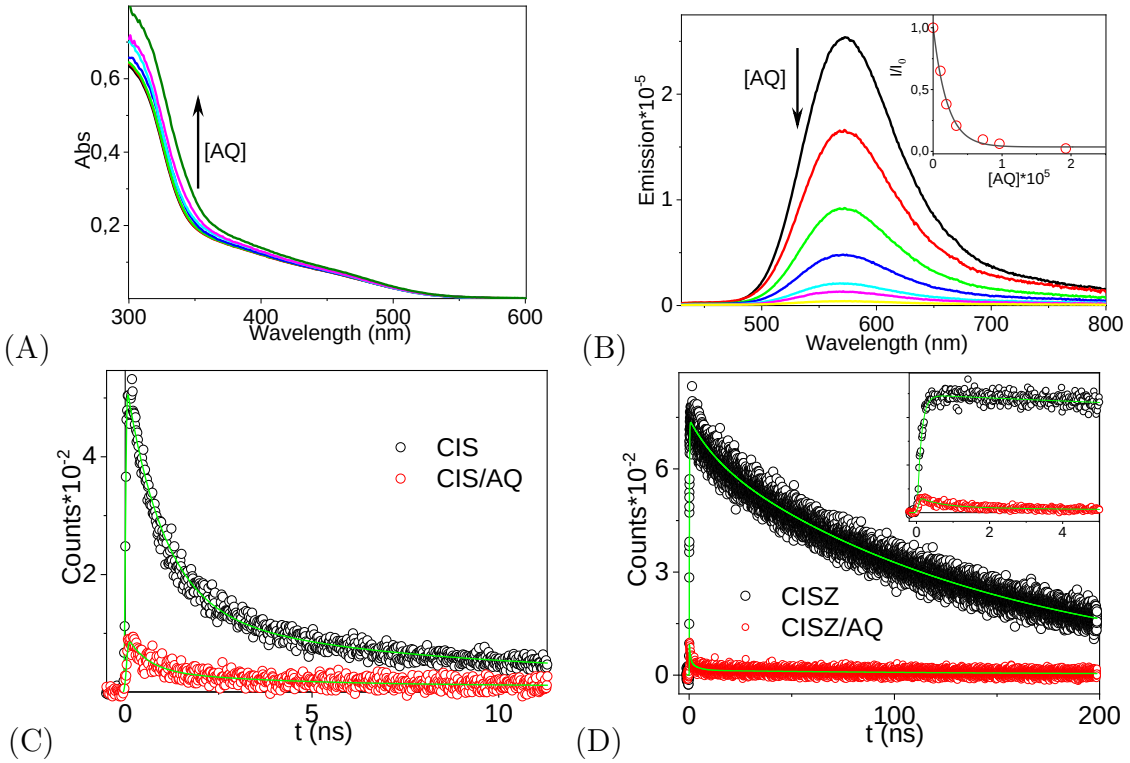

Figure 3: (A) Absorbance spectra of CISZ after adding 1.1, 1.9,3.6, 7.2, 9.6 and 19.2 µM AQ molecule. (B) Emission spectra of CISZ CS and CISZ/AQ composite with the same composition in absorbance spectra. TCSPC decay traces of CISZ CS and CISZ/AQ composite at (C) 460 nm and (D) 560 nm following 405 nm excitation.In Inset: Same traces in expanded timescale.

Figure 3 (A) shows the absorbance spectra of CISZ without and with different concentrations (1.1, 1.9,3.6, 7.2, 9.6 and 19.2 μM) of AQ in chloroform solvent, where the concentration of CISZ is kept the same for all compositions. The unchanged absorbance spectrum of CISZ after the addition of AQ molecule is attributed to the unaffected CB and VB of CISZ in the presence of AQ. The absorbance at the blue ($<$ 400 nm) increases with AQ due to the absorbance of AQ itself. To test the interaction between CISZ and AQ, we have performed the steady-state emission spectroscopy measurements without and with AQ as shown in Figure 3 (B). These measurements were carried out with the same sample compositions as for absorbance measurements presented in Figure 3 (A). The emission of CISZ is quenched in the presence of AQ and the quenching efficiency increases with the increasing concentration of AQ.

The quite strong emission quenching reveals the strong interaction between CISZ and AQ. Roughly 98 % emission quenching of CISZ is observed at the used highest concentration of AQ. We determined the exact ratio of the concentrations of [CISZ] and [AQ] by modeling emission quenching and fitting the data. We assumed statistical complex formation with the Poisson distribution of the number of AQ attached to CISZ and complete emission quenching of CISZ if at least one AQ is attached to CISZ. The fit is shown in the inset of Figure 3 (B).[29] According to the model, the 95 % quenching is achieved at ratio [CISZ]:[AQ]=1:3, which is roughly the highest ratio used.

The reason behind the emission quenching can be either e^- or energy transfer or both. But in this case, the energy transfer can be excluded, because the energy of excited donor, CISZ, is much lower than the excited state energy of the potential acceptor, AQ. This also can be concluded from the fact that there is no absorbance of AQ at > 450 nm where CISZ emits, ruling out the energy transfer process from CISZ to AQ. Therefore, we can assume that the reason for the emission quenching is the e^- transfer (ET) process.

The steady-state emission is not an effective method to study the ET or energy transfer. Therefore, the TCSPC was used to study quenching dynamics. For this purpose, CISZ/AQ composite with 95 % quenching was used and excited at 405 nm. Figure 3 (C) compares the decay traces of CISZ and CISZ/AQ composite at 460 nm measured under the same conditions, and it shows quite strong reduction of the emission intensity of CISZ/AQ composite compared to that of CISZ. This indicates a fast quenching of emission which is much faster than the time resolution of our TCSPC instrument (roughly 60 ps). Similarly, the emission at 560 nm corresponding to the trap state is much weaker for CISZ/AQ samples compared to that of CISZ as shown in Figure 3 (D).

TA spectra of CISZ and CISZ/AQ composite

The dynamics of the ET was studied by femtosecond TA spectroscopy. The CISZ and CISZ/AQ samples in chloroform were excited at 400 nm and the measurements for both

samples have been carried out at the same pump fluency which was low enough to avoid the multiple exciton generation. Figures 4 (A) and (B) present the time-resolved TA spectra of CISZ in the visible and NIR ranges, respectively, at different time delays from just after cooling 0.3 ps to 5 ns. The TA responses of CISZ/AQ sample at the same delay times are presented in Figure 4 (C) and (D). The shape of TA spectra of CISZ/AQ composite is very similar to that of CISZ at the early time scale both in the visible and NIR. These spectra correspond to the state formed right after excitation with e^- promoted to the CB and h^+ left in the VB respectively, which is the same for both samples.

There is no apparent difference between the samples in the TA response evolution in the NIR range. For both samples the PIA spectra are featureless and show some decay with time. However, the bleach in the BE region recovers much faster for the CISZ/AQ sample.

A distinct feature of the CISZ/AQ sample TA response is the absorption band with broad maximum close to 600 nm, which becomes visible at a few tens of ps delay and later. We compare the spectra of CISZ and CISZ/AQ at 0.3 ps and 3 ns to highlight the new band arising in CISZ/AQ as shown in Figure 4 (C) inset. The band can be attributed to the AQ^- due to the ET from CISZ.[30–32] Interestingly, the spectral shape turns to positive absorbance from a bleach at 425 nm which is also a characteristic of AQ^-.

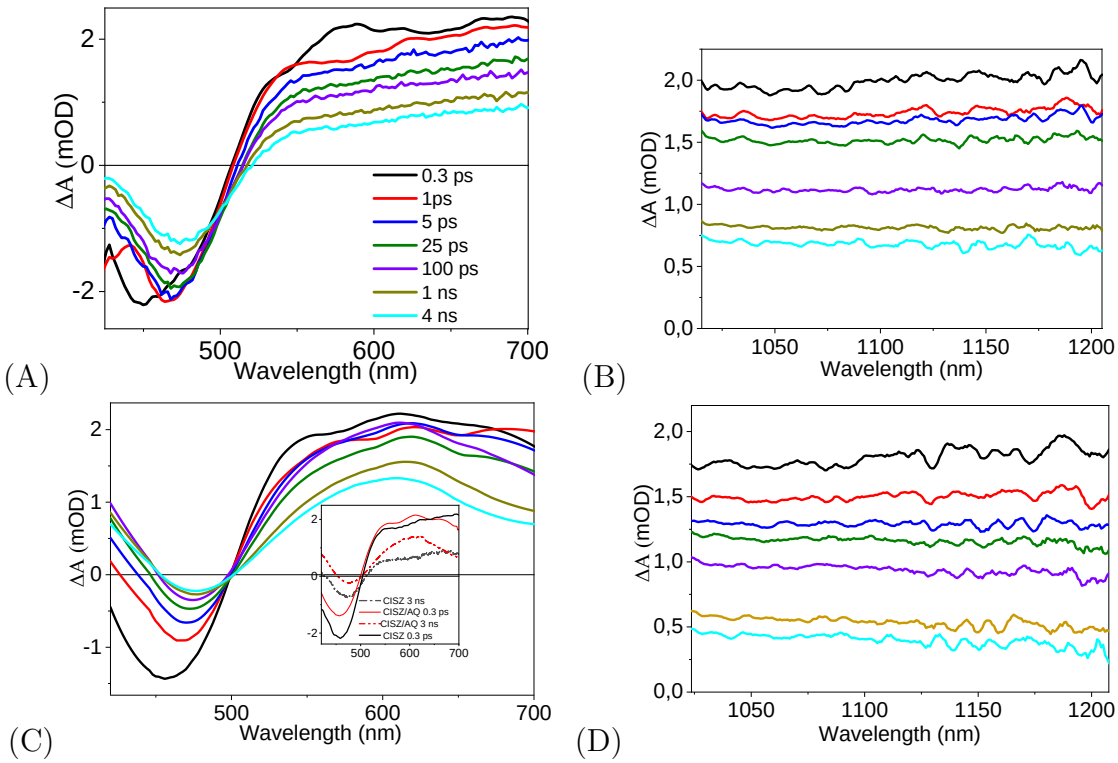

Figure 4: TA spectra of CISZ in the (A) visible and (B) NIR range. TA spectra of CISZ/AQ composite in (C) visible and (D) NIR range following 400 nm pulse excitation in chloroform medium.

In order to identify better the intermediate states and reactions between them, the TA data were fitted globally for each sample and the fit results are presented in Figure 5. In both cases, the fit included a fast component with a time constant of around 0.1 ps which was attributed to carrier cooling and not shown in the figure. In addition to this fast component, the fit model for CISZ sample included an exponent with time constant 2.3 ps (denoted as "exp(2.3 ps)" in Figure 5 (A)), a distributed decay component with average time constant 210 ps (denoted as "Gdist(210 ps)" in the figure), and a step-function (denoted as "Step" in the figure) which models a long-lived state not decaying within monitoring range of the TA system (roughly 5 ns). This was the minimum number of components that gave random residuals. We found that the minimum number of fit components for CISZ/AQ sample is also three, but the exponential component had to be replaced by distributed decay and the time constants for the CISZ/AQ sample differ from those of CISZ significantly.

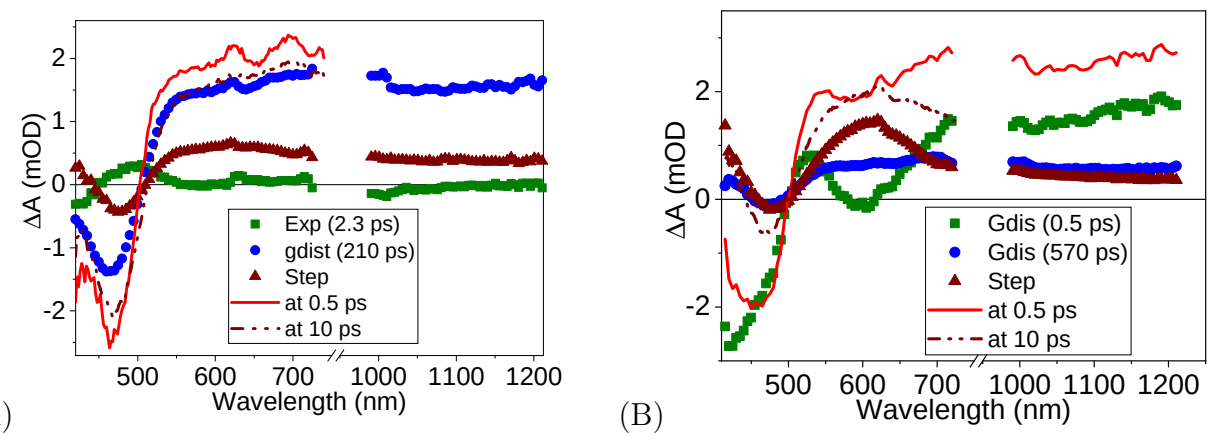

Figure 5: Transient absorption DAS and time-resolved spectra of decays of (A) CISZ and (B) CISZ-AQ.

The fast exponential component (2.3 ps) of the CISZ sample is relatively weak, its main contribution is in the BE wavelength region, and it can be attributed to the "tail" of the carriers cooling, which is essentially a non-exponential process. We cannot exclude shallow trapping–de-trapping of e^- which may result in an equilibrium between e^- in the CB and at shallow traps, but we have no experimental evidence of shallow trap state on the overall photophysics of CISZ QDs. The 210 ps component is associated with the recovery of the BE beach and the decay of PIA in the red–NIR range. It also shows some reshaping of the red-NIR absorption and can be attributed to two competing reactions, e^--h^+ recombination at CB and VB, respectively (k_{eh} in Figure 2) and h^+ trapping by defects (k_{ht}). It ends when all h^+ are trapped, but the competing recombination reduces the population of e^- at the CB. The time constant determined for this process from the emission decay measurements is 310 ps (Figure 1), which is longer than the time constant obtained from TA measurements, 210 ps. It can be suggested that the limited time resolution of the TCSPC method and the non-exponential nature of the process is the reason for the discrepancy.

The hole trapping process in our CISZ QDs is quite slower than that in many Cu-doped II-VI QDs.[33–35] CISZ is not a doped material and Cu is an integral component of the composite, and the Cu ratio is significantly higher compared to doped materials. Photoluminescence of CISZ involves holes trapped at so-called self-trap states induced by the stoichiometry of

two different cations and associated with Cu^{1+} site,[20] which differs them intentional traps induced by Cu-doping of II-VI QSs.

The long-lived component ("Step") can be associated with recombination of e^- and h^+ at the CB and defect states, respectively. This process is denoted at k_{ht} in Figure 2, and its time constant is 125 ns according to the emission decay measurements, which is much longer than the time range of the TA instrument.

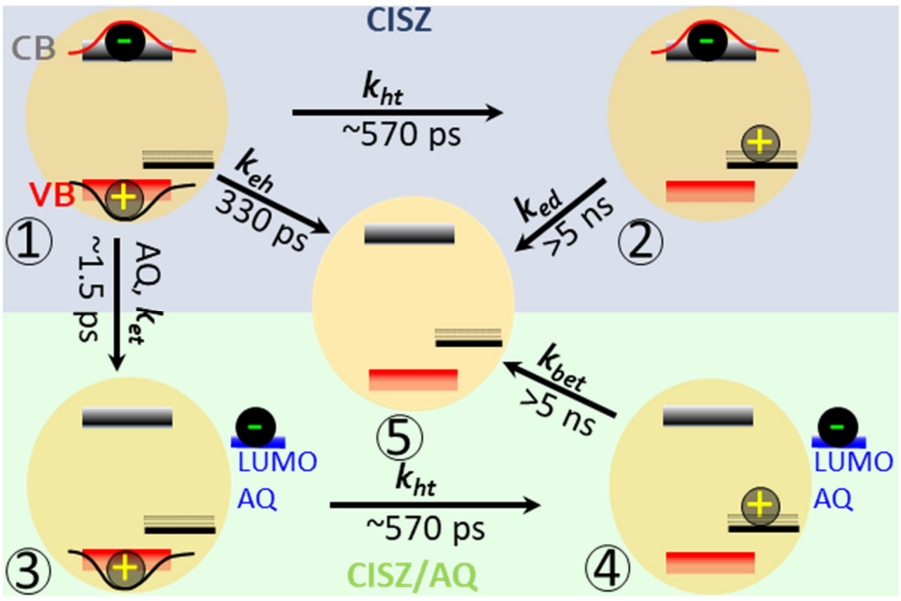

Figure 6: Schematic presentation of consecutive steps of photophysical processes in CISZ without (the top part of the scheme) and with AQ (the bottom part) after photoexcitation. All key processes HT (steps 1 to 2 and 3 to 4), ET (step 1-3), band edge recombination (step 1 to 5), trap recombination (step 2 to 5), and BET (step 4 to 5) are shown here.

The DAS and the spectra for intermediate states can be explained qualitatively by the reaction scheme in Figure 6. State 1 is presented by the spectrum at 0.5 ps in Figure 5 (A), where the e^- and h^+ are at CB and VB, respectively. Actually, the minor process with 2.3 ps time constant results in a very minor spectral changes. The time resolved spectrum after completion of this process ("at 10 ps") is shown by the dotted line in Figure 5 (A). We

will ignore this reaction in the following discussion.

The state 1 in Figure 6 has two relaxation pathways, the e^--h^+ recombination and the h^+ transfer to the defect state. The average lifetime of the state is $\tau_1 = (k_{eh} + k_{ht})^{-1} \approx 210$ ps according to TA fit results. At a few ns delay time the system is in state 2 completely. The state 2 is characterized by e^- at the CB and h^+ at defect states, respectively, as shown by the spectrum of the step function in Figure 5 (A). It relaxes to state 5 very slowly and can not be detected in TA measurements. It can be noted that amplitude of the spectrum attributed to the state 2 is much lower than that of the state 1, though it can be expected that the main contribution to both spectra comes from the e^- at CB. This indicates that the yield of the state 2 is less than half and more than half of the state 1 relax via e^-- h^+ recombination (k_{eh}). This will be discussed later.

The addition of the e^- acceptor, AQ, adds a fast, roughly 0.5 ps, reaction (Figure 5 (B)) which is characterized by gradual recovery of the BE bleach, some decay of PIA in the NIR region and formation of a band around 600 nm. These all are characteristic features of the ET from CB of QD to AQ, shown by conversion from state 1 to state 3 in Figure 6 bottom. Therefore, the ET time scale is found to be 0.5 ps and it will be 1.5 ps for one-to-to CISZ and AQ interaction as the studied composition was 1:3 ratio of CISZ and AQ. This is surprisingly fast ET but it is comparable to previously reported picosecond ET in QD-AQ hybrids.[36] A short linker connecting the donor and acceptor and favorable ET energetics are towo reasons for the fast ET. This ET is much faster than the combined CB e^--VB h^+ recombination (k_{eh}) and h^+ trapping (k_{ht}) and dominates in removing e^- from the CB. The latter is in agreement with the observed much lower emission intensity of the CISZ/AQ sample at 460 nm (BE region) as compared to CISZ samples.

There is a 570 ps component in the TA evolution of CISZ/AQ sample. The corresponding reaction can be attributed to h^+ trapping by the defect states, since its shape is similar to that of 210 ps component in the case of CISZ, and there are no signs of AQ being involved. This process does not compete with e^--h^+ recombination in CISZ/AQ sample since e^-

at CB transferred to AQ much faster. Therefore it can be assigned to k_{ht} rate constant, thus $k_{ht}^{-1} \approx 570$ ps. Since relaxation of the state 1 of CISZ was attributed to two competing reactions and its time constant $(k_{eh}+k_{ht})^{-1} \approx 210$ ps, the e^--h^+ recombination time constant can be estimated to be $k_{eh}^{-1} \approx 330$ ps. This implies that roughly 63% of states 1 relax by the recombination (to state 5), and the rest 37% yield state 2, h^+ trapped by the defect. This is in good agreement with the observation that the long-lived component (Step, state 2) of CISZ is roughly three times lower in intensity than the initially formed (at 10 ps) state 1.

The long-lived component (Step) of CISZ/AQ sample has higher intensity and distinct features of the charge-separated state 4, $CISZ^+/AQ^-$. Its lifetime is much longer than the TA monitoring time scale (roughly 5 ns), and cannot be determined with the instrument used. The spectrum of the step function component presents the final state where e^- and h^+ are at the AQ LUMO and the QD trap state, respectively, as shown by state 4 in Figure 6. Eventually, state 4 will decay to state 5 through the recombination of AQ^- and the h^+ in the QD. This process is more than 10 000 times slower than the ET, which is very unusual.

It can be noted, that in a typical QD-molecular acceptor system, the ET involves the transfer at the CB and leaves the h^+ in the VB, and the back ET is the recombination of the e^- at acceptor and the h^+ at VB. In case of CISZ/AQ system, shortly after the ET, the h^+ is trapped by the Cu^{1+} center, and recombination must involve the trapped h^+ but not the VB h^+. The rate of the ET (or BET) depends on the electronic overlap integral. The h^+ at VB of QDs are well delocalized but the trapped h^+ are mostly localized at defect sites. The h^+ localization, and thus smaller overlap integral, is the most probable reason for much slower BET in the case of CISZ/AQ hybrids. However, a similarly long-lived charge-separated state was reported previously for other QDs/molecule composites.[30,31,37,38]

Conclusion

Our study of CISZ QDs comes in agreement with previous reports suggesting that the broad and red-shifted emission is the result of recombination of the e^- at the CB and h^+ trapped at the defect sites. Furthermore, we were able to identify direct emission due to CB-VB charge recombination and estimate the time constants of the direct recombination and h^+ trapping, 330 and 570 ps, respectively. The direct recombination can be effectively eliminated by attaching e^- acceptor to the QDs, anthraquinone (AQ) derivative in our case. We observed a fast e^- transfer from the photo-excited CISZ QD to AQ, and estimated the time constant of the ET to be roughly 1.5 ps in an ideal one-to-one CISZ-AQ complex. Unexpectedly, the lifetime of the charge separated state is very long, being much greater than the maximum delay time of our TA instrument, 5 ns. We attributed this to relatively fast h^+ trapping, which results in h^+ localization at defect sites and effectively decouple e^- at AQ and h^+ at QD.

Acknowledgement

This project is supported by Jane & Aatos Erkko foundation (JAES/LACOR-31228007701).

Supporting Information Available

"All the TCSPC decay kinetics and equation for fitting. The class will automatically add a sentence pointing to the information on-line:

References

(1) Pietryga, J. M.; Park, Y.-S.; Lim, J.; Fidler, A. F.; Bae, W. K.; Brovelli, S.; Klimov, V. I. Spectroscopic and Device Aspects of Nanocrystal Quantum Dots. *Chem. Rev. 116*,

10513–10622.

(2) Arcudi, F.; Dordjević, L.; Nagasing, B.; Stupp, S. I.; Weiss, E. A. Quantum Dot-Sensitized Photoreduction of CO_2 in Water with Turnover Number > 80,000. *J. Am. Chem. Soc.* **2021**, *143*, 18131–18138.

(3) Fu, B.; Deng, C.; Yang, L. Efficiency Enhancement of Solid-State $CuInS_2$ Quantum Dot-Sensitized Solar Cells by Improving the Charge Recombination. *Nanoscale Res. Lett.* **2019**, *14*, 198.

(4) Zhou, Y.; Hu, W.; Ludwig, J.; Huang, J. Exceptionally Robust $CuInS_2$/ZnS Nanoparticles as Single Component Photocatalysts for H_2 Evolution. *J. Phys. Chem. C* **2017**, *121*, 19031–19035.

(5) Pan, Z.; Mora-Seró, I.; Shen, Q.; Zhang, H.; Li, Y.; Zhao, K.; Wang, J.; Zhong, X.; Bisquert, J. High-Efficiency "Green" Quantum Dot Solar Cells. *J. Am. Chem. Soc.* **2014**, *136*, 9203–9210.

(6) Guo, W.; Sun, X.; Jacobson, O.; Yan, X.; Min, K.; Srivatsan, A.; Niu, G.; Kiesewetter, D. O.; Chang, J.; Chen, X. Intrinsically Radioactive [64Cu]CuInS/ZnS Quantum Dots for PET and Optical Imaging: Improved Radiochemical Stability and Controllable Cerenkov Luminescence. *ACS Nano* **2015**, *9*, 488–495.

(7) Hinterding, S. O. M.; Mangnus, M. J. J.; Prins, P. T.; Jöbsis, H. J.; Busatto, S.; Vanmaekelbergh, D.; de Mello Donega, C.; Rabouw, F. T. Unusual Spectral Diffusion of Single $CuInS_2$ Quantum Dots Sheds Light on the Mechanism of Radiative Decay. *Nano Lett.* **2021**, *21*, 658–665.

(8) van der Stam, W.; de Graaf, M.; Gudjonsdottir, S.; Geuchies, J. J.; Dijkema, J. J.; Kirkwood, N.; Evers, W. H.; Longo, A.; Houtepen, A. J. Tuning and Probing the Distribution of Cu^+ and Cu_2^+ Trap States Responsible for Broad-Band Photoluminescence in $CuInS_2$ Nanocrystals. *ACS Nano* **2018**, *12*, 11244–11253.

(9) Sun, J.; Zhu, D.; Zhao, J.; Ikezawa, M.; Wang, X.; Masumoto, Y. Ultrafast carrier dynamics in $CuInS_2$ quantum dots. *Appl. Phys. Lett.* **2014**, *104*, 023118.

(10) Hamanaka, Y.; Kuzuya, T.; Sofue, T.; Kino, T.; Ito, K.; Sumiyama, K. Defect-induced photoluminescence and third-order nonlinear optical response of chemically synthesized chalcopyrite $CuInS_2$ nanoparticles. *Chem. Phys. Lett.* **2008**, *466*, 176–180.

(11) Hu, W.; Ludwig, J.; Pattengale, B.; Yang, S.; Liu, C.; Zuo, X.; Zhang, X.; Huang, J. Unravelling the Correlation of Electronic Structure and Carrier Dynamics in $CuInS_2$ Nanoparticles. *J. Phys. Chem. C* **2018**, *122*, 974–980.

(12) Eliasson, N.; Rimgard, B. P.; Castner, A.; Tai, C.-W.; Ott, S.; Tian, H.; Hammarström, L. Ultrafast Dynamics in Cu-Deficient $CuInS_2$ Quantum Dots: Sub-Bandgap Transitions and Self-Assembled Molecular Catalysts. *J. Phys. Chem. C* **2021**, *125*, 14751–14764.

(13) Kraatz, I. T.; Booth, M.; Whitaker, B. J.; Nix, M. G. D.; Critchley, K. Sub-Bandgap Emission and Intraband Defect-Related Excited-State Dynamics in Colloidal $CuInS_2$/ZnS Quantum Dots Revealed by Femtosecond Pump–Dump–Probe Spectroscopy. *J. Phys. Chem. C* **2014**, *118*, 24102–24109.

(14) Szymura, M.; Duda, M.; Karpińska, M.; Kazimierczuk, T.; Minikayev, R.; Sobczak, K.; Parlińska-Wojtan, M.; Kłopotowski, Ł. Low-Temperature Photoluminescence Dynamics Reveal the Mechanism of Light Emission by Colloidal $CuInS_2$ Quantum Dots. *J. Phys. Chem. C* **2023**, *127*, 6768–6776.

(15) Houtepen, A. J.; Hens, Z.; Owen, J. S.; Infante, I. On the Origin of Surface Traps in Colloidal II–VI Semiconductor Nanocrystals. *Chem. Mat.* **2017**, *29*, 752–761.

(16) Ueng, H. Y.; Hwang, H. L. The defect structure of $CuInS_2$. part I: Intrinsic defects. *J. Phys. Chem. Solids* **1989**, *50*, 1297–1305.

(17) Kolny-Olesiak, J.; Weller, H. Synthesis and Application of Colloidal $CuInS_2$ Semiconductor Nanocrystals. *ACS Appl. Mater. Interfaces* **2013**, *5*, 12221–12237.

(18) Xia, C.; Wu, W.; Yu, T.; Xie, X.; van Oversteeg, C.; Gerritsen, H. C.; de Mello Donega, C. Size-Dependent Band-Gap and Molar Absorption Coefficients of Colloidal $CuInS_2$ Quantum Dots. *ACS Nano* **2018**, *12*, 8350–8361.

(19) Zhong, H.; Zhou, Y.; Ye, M.; He, Y.; Ye, J.; He, C.; Yang, C.; Li, Y. Controlled Synthesis and Optical Properties of Colloidal Ternary Chalcogenide $CuInS_2$ Nanocrystals. *Chem. Mat.* **2008**, *20*, 6434–6443.

(20) Fuhr, A. S.; Yun, H. J.; Makarov, N. S.; Li, H.; McDaniel, H.; Klimov, V. I. Light Emission Mechanisms in $CuInS_2$ Quantum Dots Evaluated by Spectral Electrochemistry. *ACS Photonics* **2017**, *4*, 2425–2435.

(21) Roy, P.; Mukherjee, A.; Mondal, P.; Bhattacharyya, B.; Narayan, A.; Pandey, A. Electronic Structure and Spectroscopy of I–III–VI2 Nanocrystals: A Perspective. *J. Phys. Chem. C* **2022**, *126*, 7364–7373.

(22) Jara, D. H.; Stamplecoskie, K. G.; Kamat, P. V. Two Distinct Transitions in $CuxInS_2$ Quantum Dots. Bandgap versus Sub-Bandgap Excitations in Copper-Deficient Structures. *J. Phys. Chem. Lett.* **2016**, *7*, 1452–1459.

(23) Berends, A. C.; Rabouw, F. T.; Spoor, F. C. M.; Bladt, E.; Grozema, F. C.; Houtepen, A. J.; Siebbeles, L. D. A.; de Mello Donegá, C. Radiative and Nonradiative Recombination in $CuInS_2$ Nanocrystals and CuInS2-Based Core/Shell Nanocrystals. *J. Phys. Chem. Lett.* **2016**, *7*, 3503–3509.

(24) Jeong, S.; Ko, M.; Jeong, S.; Shin, S. Y.; Park, S. M.; Do, Y. R.; Song, J. K. Optical Transitions of $CuInS_2$ Nanoparticles: Two Types of Absorption and Two Types of Emission. *J. Phys. Chem. C* **2020**, *124*, 14400–14408.

(25) Lian, S.; Kodaimati, M. S.; Dolzhnikov, D. S.; Calzada, R.; Weiss, E. A. Powering a CO_2 Reduction Catalyst with Visible Light through Multiple Sub-picosecond Electron Transfers from a Quantum Dot. *J. Am. Chem. Soc* **2017**, *139*, 8931–8938.

(26) Xie, R.; Rutherford, M.; Peng, X. Formation of High-Quality I-III-VI Semiconductor Nanocrystals by Tuning Relative Reactivity of Cationic Precursors. *J. Am. Chem. Soc* **2009**, *131*, 5691–5697.

(27) Li, L.; Pandey, A.; Werder, D. J.; Khanal, B. P.; Pietryga, J. M.; Klimov, V. I. Efficient Synthesis of Highly Luminescent Copper Indium Sulfide-Based Core/Shell Nanocrystals with Surprisingly Long-Lived Emission. *J. Am. Chem. Soc* **2011**, *133*, 1176–1179.

(28) Zhong, H.; Bai, Z.; Zou, B. Tuning the Luminescence Properties of Colloidal I–III–VI Semiconductor Nanocrystals for Optoelectronics and Biotechnology Applications. *J. Phys. Chem. Lett.* **2012**, *3*, 3167–3175.

(29) Song, N.; Zhu, H.; Jin, S.; Zhan, W.; Lian, T. Poisson-Distributed Electron-Transfer Dynamics from Single Quantum Dots to C_{60} Molecules. *ACS Nano* **2011**, *5*, 613–621.

(30) Zhu, H.; Song, N.; Lian, T. Wave Function Engineering for Ultrafast Charge Separation and Slow Charge Recombination in Type II Core/Shell Quantum Dots. *J. Am. Chem. Soc.* **2011**, *133*, 8762–8771.

(31) Mandal, S.; George, L.; Tkachenko, N. V. Charge transfer dynamics in $CsPbBr_3$ perovskite quantum dots–anthraquinone/fullerene (C_{60}) hybrids. *Nanoscale* **2019**, *11*, 862–869.

(32) Wang, H.; Sukhanov, A. A.; Iagatti, A.; Bussotti, L.; Zhao, X.; Zhao, J.; Voronkova, V. K.; Di Donato, M. Long-Lived Charge Separated States in Anthraquinone-Phenothiazine Dyads: Synthesis and Study of the Photophysical Property by Using Transient Optical and Magnetic Resonance Spectroscopies. *Chem.Euro. J.* **2023**, *29*, e202301125.

(33) Hughes, K. E.; Hartstein, K. H.; Gamelin, D. R. Photodoping and Transient Spectroscopies of Copper-Doped CdSe/CdS Nanocrystals. *ACS Nano* **2018**, *12*, 718–728.

(34) Harchol, A.; Barak, Y.; Hughes, K. E.; Hartstein, K. H.; Jöbsis, H. j.; Prins, P. T.; de Mello Donegá, C.; Gamelin, D. R.; Lifshitz, E. Optically Detected Magnetic Resonance Spectroscopy of Cu-Doped CdSe/CdS and $CuInS_2$ Colloidal Quantum Dots. *ACS Nano* **2022**, *16*, 12866–12877.

(35) Maiti, S.; Dana, J.; Jadhav, Y.; Debnath, T.; Haram, S. K.; Ghosh, H. N. Electrochemical Evaluation of Dopant Energetics and the Modulation of Ultrafast Carrier Dynamics in Cu-Doped CdSe Nanocrystals. *The Journal of Physical Chemistry C* **2017**, *121*, 27233–27240, Publisher: American Chemical Society.

(36) Zhu, H.; Song, N.; Lian, T. Wave Function Engineering for Ultrafast Charge Separation and Slow Charge Recombination in Type II Core/Shell Quantum Dots. *J. Am. Chem. Soc.* **2011**, *133*, 8762–8771.

(37) Wu, K.; Liang, G.; Shang, Q.; Ren, Y.; Kong, D.; Lian, T. Ultrafast Interfacial Electron and Hole Transfer from $CsPbBr_3$ Perovskite Quantum Dots. *J. Am. Chem. Soc.* **2015**, *137*, 12792–12795.

(38) Boulesbaa, A.; Issac, A.; Stockwell, D.; Huang, Z.; Huang, J.; Guo, J.; Lian, T. Ultrafast Charge Separation at CdS Quantum Dot/Rhodamine B Molecule Interface. *J. Am. Chem. Soc.* **2007**, *129*, 15132–15133.

TOC Graphic

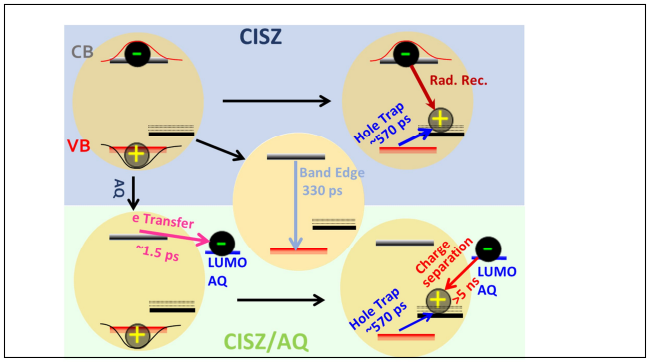

Some journals require a graphical entry for the Table of Contents. This should be laid out "print ready" so that the sizing of the text is correct.

Inside the `tocentry` environment, the font used is Helvetica 8 pt, as required by *Journal of the American Chemical Society*.

The surrounding frame is 9 cm by 3.5 cm, which is the maximum permitted for *Journal of the American Chemical Society* graphical table of content entries. The box will not resize if the content is too big: instead it will overflow the edge of the box.

This box and the associated title will always be printed on a separate page at the end of the document.